
Aligning LLMs with Biomedical Knowledge using Balanced Fine-Tuning

Zhenchao Tang^{1†,2}, Fang Wang^{1†*}, Haohuai He^{1,3}, Jiale Zhou^{1,4}, Tianxu Lv¹, Jun Zhu¹,
Shouzhi Chen¹, Minghao Yang¹, Yu Wang¹, Jiayang Wu¹, Yidong Song¹,
Yaokun Li², Jiehui Huang², Dawei Huang¹, Zhi Song¹, Jianhua Yao^{1*}

1. Tencent AI for Life Sciences Lab, Shenzhen, China.
2. DenseAI, Shenzhen, China.
3. The Hong Kong Polytechnic University, Hong Kong SAR, China.
4. Westlake University, Hangzhou, China.

[†]Equal contribution

^{*}Corresponding author

Abstract

Aligning Large Language Models (LLMs) with biomedical knowledge requires understanding both concepts and causal mechanisms in scientific reports. Supervised Fine-Tuning (SFT) often fails to capture these logical structures, while Reinforcement Learning (RL) is limited by sparse reward signals. We propose Balanced Fine-Tuning (BFT), a dual-scale post-training method that stabilizes training via confidence-weighted token-level optimization and adaptively emphasizes knowledge-dense hard samples using minimum group confidence. Experiments on medical and biological reasoning benchmarks show that BFT consistently outperforms SFT and achieves competitive or superior performance to specialized systems such as GeneAgent. Beyond improving generative accuracy, BFT enhances the fidelity of LLM-generated biomedical entity descriptions, such that their embeddings produced by standard encoders outperform those from domain-specific biological foundation models. This enables a single post-trained LLM to support both reasoning generation and representation-based biological analysis. Overall, BFT provides a concise and effective framework for aligning LLMs with biomedical knowledge while bridging generative and representational capabilities.

1 Introduction

Post-training serves as the critical bridge for aligning Large Language Models (LLMs) with specialized biomedical knowledge. While standard strategies like Supervised Fine-Tuning (SFT) and Reinforcement Learning (RL) have driven rapid advancements in general domains [1], they face unique and severe impediments in biomedicine. Biomedical texts exhibit long causal chains, dense factual dependencies, and a high prevalence of low-frequency but semantically critical entities (e.g., genes, proteins, pathways, and phenotypes). Capturing such structure requires more than surface-level pattern matching: models must internalize both conceptual relationships and mechanistic logic embedded in scientific reports. Standard SFT tends to optimize surface-level linguistic plausibility, memorizing high-frequency patterns without internalizing underlying biological logic. Conversely,

*Corresponding author to: Fang Wang (avonwanghit@gmail.com), Jianhua Yao (jianhua.yao@gmail.com)

RL is restricted by the absence of effective reward signals, which often require wet-lab feedback and cannot be reliably approximated by heuristic proxies [2, 3, 4].

To mitigate the instability and overfitting inherent in SFT, methods such as Dynamic Fine-Tuning (DFT) [5] stabilize training by globally down-weighting tokens with low prediction probabilities. However, this approach relies on the simplified assumption that all low-probability predictions constitute noise. To investigate the nature of these signals in a reasoning context, we performed a hierarchical analysis on samples from a biomedical QA corpus [6] using the base model. Specifically, we evaluated the next-token prediction probability $\pi_\theta(y_t^* | y_{<t}^*, x)$ for each token in the reference answer. Our analysis reveals a critical dichotomy in uncertainty types (Figure 1).

We distinguish these signals based on their temporal persistence. Group A corresponds to isolated low-confidence events, operationalized as a local 10-token context centered on a single token with $\pi < 0.1$ and flanked by high-probability neighbors, capturing transient, non-structural uncertainty. In contrast, Group B consists of sustained low-confidence spans, identified using a local 10-token sliding window where the average probability $\bar{\pi} < 0.15$. While both groups are analyzed at the same local window scale, Group A lacks temporal persistence, whereas Group B exhibits coherent low-confidence structure. Empirically, Group A is dominated by interchangeable expressions (e.g., near-synonymous verbs, adverbs, and discourse connectors), with a small fraction of ordinary words and only rare biomedical entities or reasoning connectives; this pattern reflects primarily aleatoric uncertainty. By contrast, Group B is dominated by biomedical entities and causal reasoning chains, with only a small amount of ordinary filler words and very few interchangeable expressions, reflecting epistemic uncertainty. To quantify the semantic composition in Figure 1, we utilized SciSpacy [7] to identify biomedical entities, while logical connectives were identified via a predefined set of causal indicators. This distinction is crucial: indiscriminately suppressing all low-confidence tokens may stabilize optimization, but it also suppresses knowledge-bearing spans and hinders long-tail biomedical learning.

To bridge this gap, we propose Balanced Fine-Tuning (BFT), a framework that reconciles stability with hard-sample acquisition. While our semantic analysis uses a narrow 10-token window to highlight local semantic composition, BFT employs a broader sliding window ($g = 256$) during training to preserve full reasoning chains. BFT introduces a dual-scale mechanism: (1) At the token level, it inherits DFT’s probability-dependent rescaling to prevent instability from isolated low-confidence tokens, which are a major source of gradient explosion in vanilla SFT. (2) At the sample level, BFT uses the *lowest group probability* in each sequence as a hard-sample signal, and applies a bounded coefficient s_b to strengthen learning on knowledge-dense samples. Because $s_b \in [0, 1]$ and is detached by stop-gradient, this enhancement is numerically controlled and does not reintroduce gradient explosion. Importantly, BFT reweights whole samples rather than local fragments, so the model is encouraged to learn coherent biomedical reasoning processes instead of overfitting to isolated spans.

Crucially, the impact of BFT extends beyond text generation. A persistent challenge in computational biology is the bifurcation of tasks [8]: generative tasks (e.g., QA) rely on LLMs, while discriminative tasks (e.g., gene interaction prediction) depend on specialized biological foundation models. We demonstrate that BFT bridges this divide by effectively transforming the LLM into a high-fidelity semantic projector. Unlike standard SFT, which often produces generic descriptions that blur the distinctions between similar biological entities, BFT’s focus on epistemic uncertainty forces the model to articulate precise causal mechanisms and specific regulatory roles. Consequently, the high-quality textual descriptions generated by the BFT-tuned LLM, when encoded by a standard text embedding model, yield embeddings that are topologically aligned with biological semantics. This results in strong generalization in downstream tasks ranging from genes to cells, effectively transforming LLMs into robust biomedical encoders without the need for specialized pre-training.

Our contributions are primarily twofold. First, in generative tasks, BFT-based models outperform SFT, DFT, and complex agents like GeneAgent [9] in terms of reasoning accuracy. Second, in discriminative tasks, the embeddings derived from BFT-generated descriptions surpass those from specialized biological foundation models such as scGPT [10] and STATE [11]. This indicates that BFT simultaneously enhances both reasoning generation capabilities and biological representation capabilities, thereby facilitating the integration of LLMs with life sciences.

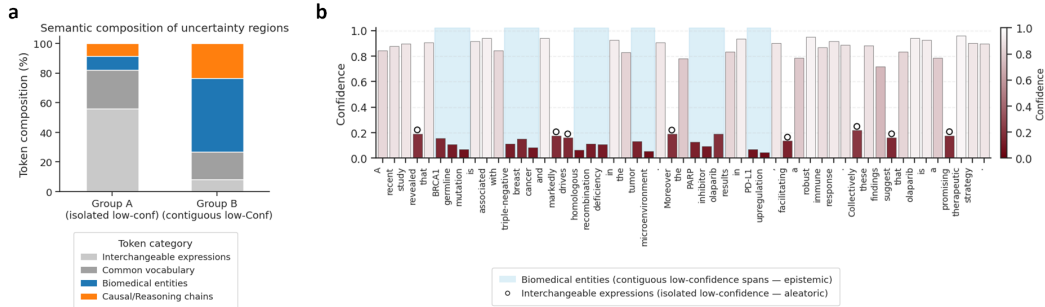


Figure 1: We distinguish isolated probability drops (Group A) from sustained low-confidence spans (Group B). **a**: Semantic composition statistics comparing Group A and Group B. Group A is mainly composed of interchangeable expressions (aleatoric uncertainty), whereas Group B is dominated by biomedical entities and reasoning/causal connectors (epistemic uncertainty). **b**: A concrete token-level visualization example. Bar color and height indicate confidence; blue shaded regions mark contiguous biomedical entity spans, and hollow-circle markers denote isolated interchangeable expressions.

2 Related Work

SFT Post-Training In the absence of dense reward signals for Reinforcement Learning, improving SFT has emerged as a primary research focus. DFT [5] represents the state-of-the-art in this field, identifying that standard SFT suffers from gradient instability due to implicit inverse probability weighting. DFT addresses this issue by rescaling the loss based on token prediction confidence, treating low-probability tokens as noise to be suppressed. Recent studies on post-training also tend to overlook explicit strengthening of hard samples, even when adopting related re-weighting strategies [12, 13, 14, 15, 16, 17, 18]. To more accurately assess reasoning reliability, DeepConf [19] introduced group confidence as a localized measurement to identify reasoning breakdowns during inference by monitoring confidence signals within a sliding window. BFT builds upon DFT’s efficient stabilization but shifts the application of localized confidence from test-time filtering to post-training alignment. Specifically, BFT utilizes a similar group confidence mechanism to identify and adaptively up-weight "hard" reasoning samples, ensuring that sustained low-confidence sequences—which represent epistemic logic rather than aleatoric noise—are prioritized during learning.

Biomedical Representation Models Acquiring embeddings for biological entities is essential for downstream tasks [20, 21, 22, 23]. Existing approaches fall into two categories. Specialized foundation models, such as scGPT [10] and Geneformer [24], are pre-trained on large-scale biological datasets but require substantial computational resources and are often modality-constrained (e.g., transcriptomics) [25]. Text-based methods, such as GenePT [26], use GPT-4o to generate textual descriptions that are then embedded (with text-embedding-ada-002), but these representations often lack domain-specific depth due to misalignment with biomedical logic. We align LLMs using BFT to generate biologically grounded descriptions, whose embeddings produced by a standard encoder capture biological semantics more faithfully.

3 Methods

3.1 Supervised Fine-Tuning (SFT)

Supervised fine-tuning (SFT) is the standard approach for aligning large language models (LLMs) with human-annotated data. Given a dataset $\mathcal{D} = \{(x, y^*)\}$ of instruction–response pairs, SFT minimizes the token-level cross-entropy loss:

$$L_{\text{SFT}}(\theta) = \mathbb{E}_{(x, y^*) \sim \mathcal{D}} \left[-\log \pi_{\theta}(y^* | x) \right], \quad (1)$$

where $\pi_{\theta}(y^* | x)$ is the model likelihood of the reference response. The gradient is:

$$\nabla_{\theta} L_{\text{SFT}}(\theta) = \mathbb{E}_{(x, y^*) \sim \mathcal{D}} \left[-\nabla_{\theta} \log \pi_{\theta}(y^* | x) \right]. \quad (2)$$

The reinforcement learning objective maximizes the expected reward:

$$J(\theta) = \mathbb{E}_{x \sim \mathcal{D}_x, y \sim \pi_{\theta}(\cdot | x)} [r(x, y)], \quad (3)$$

with the policy gradient theorem yielding:

$$\nabla_{\theta} J(\theta) = \mathbb{E}_{x \sim \mathcal{D}_x, y \sim \pi_{\theta}(\cdot | x)} [\nabla_{\theta} \log \pi_{\theta}(y | x) \cdot r(x, y)]. \quad (4)$$

Applying importance sampling to the SFT gradient:

$$\nabla_{\theta} L_{\text{SFT}}(\theta) = \mathbb{E}_{x \sim \mathcal{D}_x} \mathbb{E}_{y \sim \pi_{\theta}(\cdot | x)} \left[\frac{\delta(y, y^*)}{\pi_{\theta}(y | x)} (-\nabla_{\theta} \log \pi_{\theta}(y | x)) \right], \quad (5)$$

where $\delta(y, y^*)$ is the Kronecker Delta function (1 when $y = y^*$, 0 otherwise). Defining weight: $w(y | x) = \pi_{\theta}(y | x)^{-1}$, which reduces to $\pi_{\theta}(y^* | x)^{-1}$ since implicit reward $r_{\text{SFT}}(x, y) = \delta(y, y^*)$, yields the RL-equivalent form:

$$\nabla_{\theta} L_{\text{SFT}}(\theta) = -\mathbb{E}_{x \sim \mathcal{D}_x, y \sim \pi_{\theta}(\cdot | x)} [w(y | x) r_{\text{SFT}}(x, y) \nabla_{\theta} \log \pi_{\theta}(y | x)]. \quad (6)$$

The weight $w(y | x) = \pi_{\theta}(y^* | x)^{-1}$ introduces instability: gradient explosion when $\pi_{\theta}(y^* | x) \rightarrow 0^+$.

3.2 Dynamic Fine-Tuning (DFT)

Dynamic Fine-Tuning (DFT) [5] stabilizes SFT by rescaling each token-level loss with its predicted probability, detached from gradient flow. This directly reduces the impact of isolated low-confidence tokens that otherwise can trigger unstable large gradients in token-level cross-entropy training.

$$L_{\text{DFT}}(\theta) = \mathbb{E}_{(x, y^*) \sim \mathcal{D}} \left[\sum_{t=1}^{|y^*|} \text{sg}(\pi_{\theta}(y_t^* | y_{<t}^*, x)) \ell_t \right], \quad (7)$$

where $\ell_t = -\log \pi_{\theta}(y_t^* | y_{<t}^*, x)$ and $\text{sg}(\cdot)$ denotes the stop-gradient operator. DFT thus down-weights low-confidence tokens to stabilize optimization, but this indiscriminate suppression may also under-train difficult, knowledge-dense samples that contain epistemic uncertainty.

3.3 Balanced Fine-Tuning (BFT)

We introduce Balanced Fine-Tuning (BFT), which incorporates a sample-level confidence weighting scheme on top of Dynamic Fine-Tuning (DFT). Inspired by the group confidence mechanism from DeepConf [19], BFT first preserves DFT’s token-level stability, then selectively strengthens learning on knowledge-dense hard samples.

Per-token confidence For each token t of sample b , given logits $\mathbf{z}_{b,t} \in \mathbb{R}^V$ (V is the vocabulary size) and target token $y_{b,t}$, we define token confidence as:

$$c_{b,t} = \pi_{\theta}(y_{b,t} | y_{b,<t}, x_b) = \text{softmax}(\mathbf{z}_{b,t})[y_{b,t}]. \quad (8)$$

Group confidence We measure local reasoning reliability by averaging token confidences within a sliding window G_i of length g :

$$C_{G_i} = \frac{1}{|G_i|} \sum_{t \in G_i} c_{b,t}. \quad (9)$$

Windows are constructed with stride 1. At sequence boundaries, we adopt valid-window semantics, i.e., only windows fully contained within the sequence are considered, so that $|G_i| = g$ for all G_i . In practice, this is implemented via a 1D convolution with a uniform kernel of size g and no padding, followed by normalization by g .

Lowest group confidence The weakest region of each sequence is characterized by its lowest group confidence:

$$p_b^{\text{conf}} = \min_{G_i \in \mathcal{G}_b} C_{G_i}, \quad (10)$$

where \mathcal{G}_b denotes the set of all valid overlapping token groups of sample b , each group G_i containing g consecutive tokens (stride = 1).

Reweighting For sample-level, we define each sample’s balance coefficient as: $s_b = \text{sg}(1 - p_b^{\text{conf}})$, which scales per-sample loss inversely with model confidence. Thus, $s_b \approx 0$ for confident samples and $s_b \approx 1$ for difficult ones, while remaining strictly bounded in $[0, 1]$. The stop-gradient operator $\text{sg}(\cdot)$ prevents gradients from flowing through the sample-level confidence signal, making this enhancement numerically controlled and stable. For token-level, let $\ell_{b,t} = -\log \pi_\theta(y_{b,t} | y_{b,<t}, x_b)$ denote the token-level cross-entropy loss. Following DFT, we define the token confidence weight as:

$$w_{b,t} = \text{sg}(\pi_\theta(y_{b,t} | y_{b,<t}, x_b)) = \text{sg}(\exp(-\ell_{b,t})). \quad (11)$$

BFT objective BFT integrates token-level stabilization and sample-level reweighting:

$$\mathcal{L}_{\text{BFT}}(\theta) = \frac{1}{B} \sum_{b=1}^B s_b \frac{\sum_t m_{b,t} w_{b,t} \ell_{b,t}}{\sum_t m_{b,t} + \varepsilon}, \quad (12)$$

where B is the mini-batch size, $m_{b,t} \in \{0, 1\}$ is the validity mask, and ε is a small constant for numerical stability. All confidence-derived weights ($w_{b,t}$ and s_b) are detached from the computation graph, ensuring that BFT inherits the gradient stability properties of DFT while introducing adaptive emphasis on knowledge-dense hard samples.

Interpretation BFT unifies SFT, DFT, and confidence-weighted learning under a single framework: **SFT**: $s_b = 1, w_{b,t} = 1$; **DFT**: $s_b = 1, w_{b,t} = \text{sg}(\pi_\theta(y_{b,t} | y_{b,<t}, x_b))$; **BFT**: $s_b = \text{sg}(1 - p_b^{\text{conf}})$, $w_{b,t} = \text{sg}(\pi_\theta(y_{b,t} | y_{b,<t}, x_b))$. This formulation preserves DFT’s token-level gradient stabilization while adding bounded sample-level strengthening on underconfident, knowledge-dense samples; importantly, reweighting is applied at the whole-sample level rather than fragment level, reducing the risk of memorizing isolated spans. BFT adds one sliding-window mean per sequence (implemented via `conv1d` without padding) and one per-sample scalar weighting, remaining fully compatible with LoRA, mixed precision, and distributed training. A comparison of the algorithmic procedures for SFT and BFT is provided in Appendix A.1. The semantic mapping of Group A/B token composition is summarized in Appendix C.1.

4 Experimental Setup

4.1 Datasets

Mathematical Reasoning. We adopt mathematical reasoning as the testbed for our ablation studies, primarily for two reasons. First, the rigorous, multi-step deduction inherent in mathematics parallels the complex causal reasoning capabilities required by biomedical LLMs. Second, mathematical benchmarks enable a direct comparison between BFT and RL. This allows us to verify BFT’s ability to achieve generalization performance comparable to RL in the absence of external reward signals. We train on the **NuminaMath** dataset [27], which contains high-quality chain-of-thought solutions. Evaluation is performed on three widely used benchmarks: **Math-OAI** [28], **Minerva Math** [29], and **OlympiadBench** [30], covering a wide range of difficulty levels.

Medical Competence. For medical alignment, we utilize the OpenAI Health Bench [31]. Following the standard protocol, we use the *Consensus* subset (high expert agreement) for fine-tuning and evaluate on the *Hard* subset (ambiguous, complex cases) to test generalization. Performance is measured across theme-wise and axis-wise.

General Capabilities (Forgetting Analysis). To assess catastrophic forgetting, we evaluate models trained on medical data using MMLU [32] and CMMLU [33], ensuring that domain alignment does not compromise general intelligence.

Biological Reasoning and Representation. To evaluate biological domain alignment, we construct a specialized instruction-tuning dataset derived from NCBI text provided by GenePT [26], processed

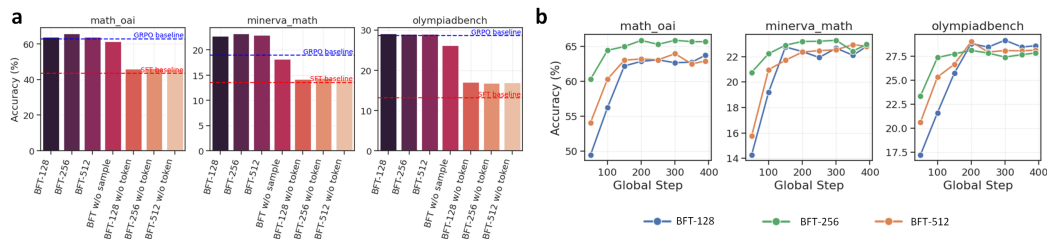


Figure 2: Ablation study. **a**: The red dashed line represents SFT, and the blue dashed line represents RL (GRPO). We test three window size (BFT-128, BFT-256, and BFT-512). BFT w/o sample denotes removing the sample-level weighting. BFT w/o token denotes removing the token-level weighting. **b**: Tracking the reasoning performance of BFT (with different window length settings) within 1 epoch.

via GPT-OSS-120B [34] into ShareGPT format. To ensure evaluation validity, we verified that downstream tasks (e.g., predicting methylation status or dosage sensitivity) target genomic properties not explicitly stated in the NCBI functional summaries. This setup forces the model to synthesize latent biological logic rather than performing simple information retrieval, ensuring the results reflect representational generalizability. For **Generative Tasks**: We evaluate biological process reasoning using benchmarks established by GeneAgent [9], reporting the ROUGE-L score. For **Representation Tasks**: We evaluate the quality of text embeddings derived from the fine-tuned models. Gene-level tasks include biological attribute prediction and interaction prediction. Cell-level tasks include phenotype clustering, cell type clustering, and single-cell multimodal integration (RNA + ADT). Finally, we test perturbation response prediction using datasets from STATE [11].

4.2 Models and Baselines

We employ the DeepSeek-R1-Distill series (1.5B, 14B, 32B, and 70B) [1] as our base models. These models possess strong initial reasoning capabilities, making them ideal for testing post-training alignment strategies. We compare BFT against the following baselines: **SFT**: The standard approach optimizing the negative log-likelihood of reference tokens. **DFT** [5]: A dynamic re-weighting method that scales loss based on token-level confidence to stabilize gradients. **Domain-Specific Models**: In biological tasks, we compare against GeneAgent [9] for reasoning, and scGPT [10], GenePT [26], and STATE [11] for representation learning tasks. A systematic overview of biomedical tasks is provided in Appendix C.2, which details the biological significance, specific domain knowledge required, and current state-of-the-art (SOTA) baselines (such as GeneAgent, GenePT, and STATE) for each task.

4.3 Implementation Details

Based on our ablation study, we set the default sliding window size to $g = 256$. All models are fine-tuned using the LlamaFactory framework [35], adopting the standard hyperparameters specified in the official Supervised Fine-Tuning (SFT) configurations. For performance assessment, we utilize domain-standardized pipelines: mathematical reasoning tasks are evaluated using Qwen2.5-Math evaluation framework [36], while medical competence benchmarks are processed through OpenAI simple-evals pipeline. For biological representation tasks, the textual responses generated by the LLMs are converted into 2048-dim vector representations using the Youtu-Embedding model [37]. All training and inference experiments are conducted on NVIDIA H20 GPUs.

5 Results

5.1 Ablation Study

We performed ablation studies on BFT using the DeepSeek-R1-Distill (1.5B) model. As shown in Figure 2a, BFT consistently outperforms SFT in mathematical reasoning and achieves performance comparable to GRPO [38]. Component analysis reveals a hierarchical dependency: token-level

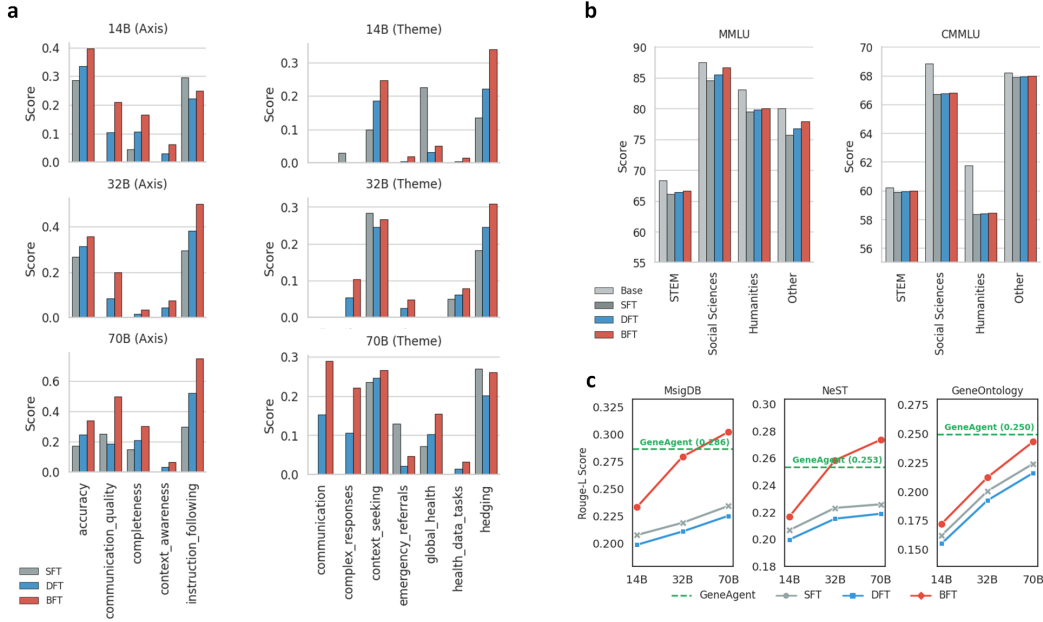


Figure 3: Text generation comparison. **a**: Medical performance is measured across axis-wise (left) and theme-wise (right). **b**: We evaluated the general capabilities of LLMs (fine-tuned on the OpenAI Health Bench *Consensus* subset) on MMLU (left) and CMMLU (right). **c**: Comparison on the biological reasoning benchmarks.

weighting is crucial for initial generalization, while sample-level weighting further boosts performance. Notably, removing token-level weighting significantly degrades results (approaching standard SFT performance), suggesting that gradient stability is a prerequisite for effective hard sample mining. Regarding hyperparameters, Figure 2b demonstrates that BFT is robust to variations in window size; we select a window size of 256 as the default to obtain relatively superior performance.

5.2 Medical Competence

We fine-tuned base models (DeepSeek-R1-Distill series 14B, 32B, and 70B) on the *Consensus* subset and evaluated them on the *Hard* subset to assess generalization to challenging medical scenarios. Health Bench adopts two complementary evaluation views: **theme-wise evaluation**, which categorizes results by medical themes, including complex_response, health_data_task, communication, and clinical knowledge; and **axis-wise evaluation**, which measures model performance across key skill dimensions such as instruction following, factual accuracy, completeness, and reasoning depth. Each score is computed based on OpenAI simple-evals that assess the quality of model outputs along multiple axes, normalized to a 0–1 range and averaged across all samples within each subset or theme. As shown in Figure 3a, BFT significantly improves the performance of LLMs on OpenAI Health Bench. BFT is superior to SFT and DFT in most aspects. In the axis-wise evaluation, BFT greatly enhances metrics such as instruction following, accuracy, and completeness. In the theme-wise evaluation, for certain themes like complex_response, health_data_task, and communication, BFT enables LLMs to master knowledge that is difficult for SFT to learn.

5.3 General Capabilities

SFT often causes LLMs to experience catastrophic forgetting, where knowledge acquired from general domains is partially lost after domain-specific fine-tuning. To assess whether domain-specific fine-tuning induces catastrophic forgetting, we evaluated the DeepSeek-R1-Distill (70B) model on widely recognized general benchmarks, MMLU [32] and CMMLU [33]. As shown in Figure 3b, while SFT leads to a regression in general capabilities, BFT consistently outperforms both SFT and

DFT, achieving scores comparable to the base model. These results indicate that BFT effectively stabilizes gradients and preserves general knowledge during domain-specific alignment, achieving the trade-off between specialization and generalization.

5.4 Biological Reasoning

In the biology domain, we fine-tuned LLMs with SFT, DFT, and BFT using ShareGPT-style data generated from NCBI gene summaries: GenePT text [26] was used as the knowledge source in EasyDataset [39], and GPT-OSS-120B [34] was used for data synthesis. Concrete training-data examples are provided in Appendix B.1.

On biological process reasoning, Figure 3c shows that BFT consistently outperforms SFT/DFT across models and datasets; DFT can underperform SFT because uniformly down-weighting low-confidence tokens suppresses low-frequency but knowledge-critical biomedical signals (e.g., TP53-like long-tail entities and relations). This supports BFT’s hard-sample emphasis and sample-level reweighting. For the strongest setting (DeepSeek-R1-Distill 70B), BFT also outperforms GeneAgent [9] in Figure 3c while avoiding external API/database dependencies and agent orchestration. For detailed qualitative evidence: case studies are shown in Appendix B.2 and B.3, with full side-by-side analyses in Appendix C.3 and C.4.

5.5 Gene-Level Representation

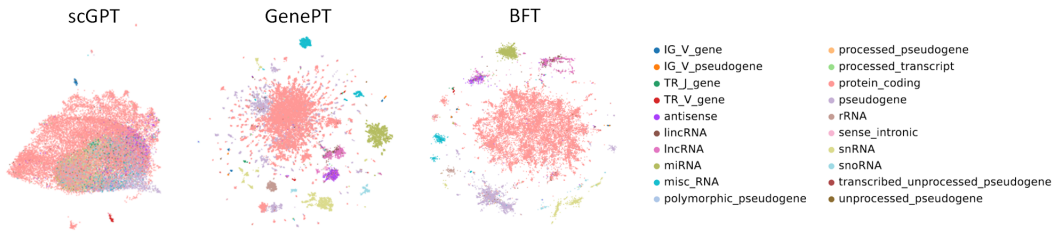


Figure 4: UMAP visualization of gene embeddings. BFT represents the text embeddings of gene descriptions output by BFT-based DeepSeek-R1-Distill 70B.

Considering that many downstream biological tasks can be accomplished through representation learning, we further examined whether the embeddings generated by BFT-based LLM capture biological knowledge. As shown in Appendix B.4, we obtained response texts from BFT-based LLM and generated their embeddings using Youtu-Embedding [37]. The UMAP visualization in Figure 4 shows that genes with similar biological functions form distinct clusters, indicating that BFT-based representations reflect biological heterogeneity at the gene level. Compared with scGPT [10] and GenePT [26], BFT-based embeddings exhibit more compact and biologically meaningful clustering.

For quantitative evaluation, we followed the benchmark established by GenePT to test two gene-level tasks. The first task predicts biological properties from a single-gene embedding, and the second predicts the interaction type from a pair of gene embeddings. As shown in Figures 5a–b, BFT-based embeddings achieve the best performance on both tasks. For multi-gene input tasks, the UMAP visualization of classifier embeddings (Appendix B.5) further demonstrates that BFT-based embeddings capture clearer biological heterogeneity. These results indicate that BFT enhances the ability of LLMs to represent biological knowledge. Regarding the results of SFT, DFT and other text encoders [40], please refer to Appendix C.5.

5.6 Cell-Level Representation

We further evaluated the potential of BFT in cell-level embedding representation. As shown in Appendix B.4, we directly obtained cell embeddings by weighted aggregation of single-cell expression data and gene embeddings. In Figure 5c-d, we evaluated the heterogeneity of cell embeddings using phenotypic labels and cell type labels respectively, and found that BFT-based embeddings perform the best. This result also reveals an interesting phenomenon: BFT-based embeddings outperform

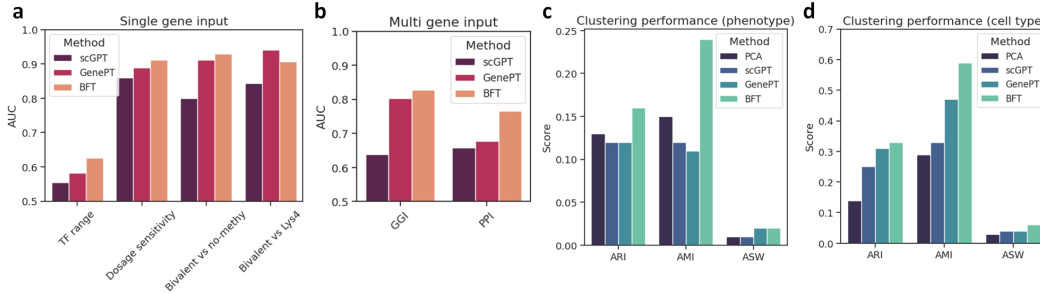


Figure 5: Representation evaluation at the gene and cell levels. **a**: Single-gene tasks: a classifier takes individual gene embeddings to predict biological attributes, including long-range vs. short-range transcription factors, dosage-sensitive vs. insensitive transcription factors, and chromatin states (bivalent, Lys4-only methylated, or non-methylated genes). **b**: Pairwise tasks: embeddings of gene or protein pairs are concatenated to predict interaction types. **c–d**: Cell-level tasks: cell embeddings are constructed by aggregating gene embeddings, and evaluated on **c**, phenotype classification and **d**, cell type annotation.

scGPT, a single-cell foundation model pre-trained with large-scale single-cell datasets. This indicates that BFT indeed has the ability to align LLMs with biological knowledge. In Appendix B.6, we used UMAP to compare the PCA embeddings of raw data and BFT-based embeddings. We found that BFT-based embeddings eliminate batch effects across patients and distinguishes clusters of different cell types. Regarding the results of SFT, DFT and other text encoders [40], please refer to Appendix C.5.

We also evaluated the single-cell multi-modal integration task [41]. We used BFT-based LLM to obtain protein texts, then used Youtu-Embedding to generate protein embeddings, and obtained cell embeddings under the protein modality in the same way. After mixing with cell embeddings under the RNA modality, we found that BFT-based embeddings have multi-modal integration ability. We compared this method with mainstream integration methods such as BBKNN [42], Harmony [43], and scMODAL [44]. The metrics were calculated using scIB [45]. The integration performance of BFT is second only to scMODAL and far exceeds that of Harmony and BBKNN (Appendix B.8). This indicates that BFT-based embeddings not only preserve biological heterogeneity but also accurately align the two modalities. For the UMAP visualization of the integration results, please refer to Appendix B.7.

BFT-based embeddings demonstrate excellent biological knowledge in cell atlases and have the potential to serve as a unified representation in virtual cells [46]. We applied BFT-based embeddings to virtual cells, where its main task is perturbation response prediction. We obtained cell embeddings by weighting the gene embeddings of BFT-based LLM, and then used these cell embeddings as the input for the STATE [11] decoder. We achieved zero-shot performance comparable to the standard STATE model across four datasets [47] (Appendix B.9). Notably, BFT attains this parity without the extensive biological data management costs mandated by specialized models, positioning it as a robust unified representation for future virtual cell research.

6 Conclusions

In this study, we propose Balanced Fine-Tuning (BFT), a dual-scale post-training method for biomedical alignment without dense reward supervision. BFT combines token-level confidence reweighting for optimization stability with bounded sample-level hard-sample emphasis, improving learning on knowledge-dense sequences while avoiding fragment-level overfitting. This design is motivated by biomedical data, where key signals are concentrated in long-tail entities and causal chains. Empirically, BFT delivers consistent gains on two fronts: stronger biological reasoning than SFT/DFT (and competitive performance versus specialized systems such as GeneAgent), and higher-quality text-derived embeddings that transfer across gene-level prediction, cell-level clustering, multimodal integration, and virtual-cell-style perturbation tasks. These results position BFT as a practical bridge

between generative reasoning and representation learning. For limitations, evaluation currently covers a limited set of benchmarks and model families, and broader validation across modalities, and laboratories is still required.

Data availability and code availability

All datasets used in this study are already published and were obtained from public data repositories. Mathematical datasets are available at [<https://github.com/yongliang-wu/DFT>]. Healthcare datasets are available at [<https://openai.com/index/healthbench/>]. NCBI texts are available at [<https://github.com/yiqunchen/GenePT>]. Biological process reasoning Benchmark are available at [<https://github.com/ncbi-nlp/GeneAgent>]. Single-cell perturbation response prediction datasets are available at [<https://github.com/ArcInstitute/state>]. The code of this study is available at <https://github.com/TencentAILabHealthcare/BFT> or <https://git.woa.com/gelseywang/BFT>.

Competing interests

The authors declare no competing interests.

References

- [1] Daya Guo, Dejian Yang, Haowei Zhang, Junxiao Song, Peiyi Wang, Qihao Zhu, Runxin Xu, Ruoyu Zhang, Shirong Ma, Xiao Bi, et al. Deepseek-r1 incentivizes reasoning in llms through reinforcement learning. *Nature*, 645(8081):633–638, 2025.
- [2] Biqing Qi, Kaiyan Zhang, Kai Tian, Haoxiang Li, Zhang-Ren Chen, Sihang Zeng, Ermo Hua, Hu Jinfang, and Bowen Zhou. Large language models as biomedical hypothesis generators: a comprehensive evaluation. *arXiv preprint arXiv:2407.08940*, 2024.
- [3] Fenglin Liu, Hongjian Zhou, Boyang Gu, Xinyu Zou, Jinfa Huang, Jinge Wu, Yiru Li, Sam S Chen, Yining Hua, Peilin Zhou, et al. Application of large language models in medicine. *Nature Reviews Bioengineering*, pages 1–20, 2025.
- [4] Yuanhao Qu, Kaixuan Huang, Ming Yin, Kanghong Zhan, Dyllan Liu, Di Yin, Henry C Cousins, William A Johnson, Xiaotong Wang, Mihir Shah, et al. Crispr-gpt for agentic automation of gene-editing experiments. *Nature Biomedical Engineering*, pages 1–14, 2025.
- [5] Yongliang Wu, Yizhou Zhou, Zhou Ziheng, Yingzhe Peng, Xinyu Ye, Xinting Hu, Wenbo Zhu, Lu Qi, Ming-Hsuan Yang, and Xu Yang. On the generalization of sft: A reinforcement learning perspective with reward rectification. *arXiv preprint arXiv:2508.05629*, 2025.
- [6] Qiao Jin, Bhuwan Dhingra, Zhengping Liu, William Cohen, and Xinghua Lu. Pubmedqa: A dataset for biomedical research question answering. In *Proceedings of the 2019 Conference on Empirical Methods in Natural Language Processing and the 9th International Joint Conference on Natural Language Processing (EMNLP-IJCNLP)*, pages 2567–2577, 2019.
- [7] Mark Neumann, Daniel King, Iz Beltagy, and Waleed Ammar. ScispaCy: Fast and Robust Models for Biomedical Natural Language Processing. In *Proceedings of the 18th BioNLP Workshop and Shared Task*, pages 319–327, Florence, Italy, August 2019. Association for Computational Linguistics.
- [8] Zhenchao Tang, Guanxing Chen, Shouzhi Chen, Haohuai He, Jiehui Huang, Tiejun Dong, Jun Zhou, Lu Zhao, Linlin You, and Calvin Yu-Chian Chen. Modal-next: Toward unified heterogeneous cellular data integration. *Information Fusion*, page 103479, 2025.
- [9] Zhizheng Wang, Qiao Jin, Chih-Hsuan Wei, Shubo Tian, Po-Ting Lai, Qingqing Zhu, Chi-Ping Day, Christina Ross, Robert Leaman, and Zhiyong Lu. Geneagent: self-verification language agent for gene-set analysis using domain databases. *Nature Methods*, pages 1–9, 2025.

- [10] Haotian Cui, Chloe Wang, Hassaan Maan, Kuan Pang, Fengning Luo, Nan Duan, and Bo Wang. scgpt: toward building a foundation model for single-cell multi-omics using generative ai. *Nature methods*, 21(8):1470–1480, 2024.
- [11] Abhinav K Adduri, Dhruv Gautam, Beatrice Bevilacqua, Alishba Imran, Rohan Shah, Mohsen Naghipourfar, Noam Teyssier, Rajesh Ilango, Sanjay Nagaraj, Mingze Dong, et al. Predicting cellular responses to perturbation across diverse contexts with state. *bioRxiv*, pages 2025–06, 2025.
- [12] Chongli Qin and Jost Tobias Springenberg. Supervised fine tuning on curated data is reinforcement learning (and can be improved). *arXiv preprint arXiv:2507.12856*, 2025.
- [13] Mingyang Liu, Gabriele Farina, and Asuman Ozdaglar. Uft: Unifying supervised and reinforcement fine-tuning. *arXiv preprint arXiv:2505.16984*, 2025.
- [14] He Zhu, Junyou Su, Peng Lai, Ren Ma, Wenjia Zhang, Linyi Yang, and Guanhua Chen. Anchored supervised fine-tuning. *arXiv preprint arXiv:2509.23753*, 2025.
- [15] Tao Liu, Taiqiang Wu, Runming Yang, Shaoning Sun, Junjie Wang, and Yujiu Yang. Profit: Leveraging high-value signals in sft via probability-guided token selection. *arXiv preprint arXiv:2601.09195*, 2026.
- [16] Hanze Dong, Wei Xiong, Deepanshu Goyal, Yihan Zhang, Winnie Chow, Rui Pan, Shizhe Diao, Jipeng Zhang, Kashun Shum, and Tong Zhang. Raft: Reward ranked finetuning for generative foundation model alignment. *arXiv preprint arXiv:2304.06767*, 2023.
- [17] Siyan Zhao, Zhihui Xie, Mengchen Liu, Jing Huang, Guan Pang, Feiyu Chen, and Aditya Grover. Self-distilled reasoner: On-policy self-distillation for large language models. *arXiv preprint arXiv:2601.18734*, 2026.
- [18] Idan Shenfeld, Mehul Damani, Jonas Hübötter, and Pulkit Agrawal. Self-distillation enables continual learning. *arXiv preprint arXiv:2601.19897*, 2026.
- [19] Yichao Fu, Xuwei Wang, Yuandong Tian, and Jiawei Zhao. Deep think with confidence. *arXiv preprint arXiv:2508.15260*, 2025.
- [20] Minsheng Hao, Jing Gong, Xin Zeng, Chiming Liu, Yucheng Guo, Xingyi Cheng, Taifeng Wang, Jianzhu Ma, Xuegong Zhang, and Le Song. Large-scale foundation model on single-cell transcriptomics. *Nature Methods*, 21(8):1481–1491, 2024.
- [21] Zhenchao Tang, Guanxing Chen, Hualin Yang, Weihe Zhong, and Calvin Yu-Chian Chen. Dsilddi: A domain-invariant substructure interaction learning for generalizable drug–drug interaction prediction. *IEEE Transactions on Neural Networks and Learning Systems*, 35(8):10552–10560, 2023.
- [22] Zhenchao Tang, Haohuai He, Shouzhi Chen, Jun Zhu, Tianxu Lv, Jiale Zhou, Jiehui Huang, Guanxing Chen, Linlin You, and Calvin Yu-Chian Chen. scprototransformer: Scalable reference mapping across molecules, cells and donors. *bioRxiv*, pages 2025–12, 2025.
- [23] Zhenchao Tang, Jiehui Huang, Guanxing Chen, and Calvin Yu-Chian Chen. Comprehensive view embedding learning for single-cell multimodal integration. In *Proceedings of the AAAI Conference on Artificial Intelligence*, volume 38, pages 15292–15300, 2024.
- [24] Christina V Theodoris, Ling Xiao, Anant Chopra, Mark D Chaffin, Zeina R Al Sayed, Matthew C Hill, Helene Mantineo, Elizabeth M Brydon, Zexian Zeng, X Shirley Liu, et al. Transfer learning enables predictions in network biology. *Nature*, 618(7965):616–624, 2023.
- [25] Zhenchao Tang, Fang Wang, Fan Yang, Jiangning Song, Calvin Yu-Chian Chen, and Jianhua Yao. sctransmil bridges patient-level phenotypes and single-cell transcriptomics for cancer screening and heterogeneity inference. *bioRxiv*, pages 2025–04, 2025.
- [26] Yiqun Chen and James Zou. Simple and effective embedding model for single-cell biology built from chatgpt. *Nature biomedical engineering*, 9(4):483–493, 2025.

- [27] Jia LI, Edward Beeching, Lewis Tunstall, Ben Lipkin, Roman Soletskyi, Shengyi Costa Huang, Kashif Rasul, Longhui Yu, Albert Jiang, Ziju Shen, Zihan Qin, Bin Dong, Li Zhou, Yann Fleureau, Guillaume Lample, and Stanislas Polu. Numinamath. *Hugging Face repository*, 2024.
- [28] Dan Hendrycks, Collin Burns, Saurav Kadavath, Akul Arora, Steven Basart, Eric Tang, Dawn Song, and Jacob Steinhardt. Measuring mathematical problem solving with the math dataset. *arXiv preprint arXiv:2103.03874*, 2021.
- [29] Aitor Lewkowycz, Anders Andreassen, David Dohan, Ethan Dyer, Henryk Michalewski, Vinay Ramasesh, Ambrose Slone, Cem Anil, Imanol Schlag, Theo Gutman-Solo, et al. Solving quantitative reasoning problems with language models. *Advances in neural information processing systems*, 35:3843–3857, 2022.
- [30] Chaoqun He, Renjie Luo, Yuzhuo Bai, Shengding Hu, Zhen Thai, Junhao Shen, Jinyi Hu, Xu Han, Yujie Huang, Yuxiang Zhang, et al. Olympiadbench: A challenging benchmark for promoting agi with olympiad-level bilingual multimodal scientific problems. In *Proceedings of the 62nd Annual Meeting of the Association for Computational Linguistics (Volume 1: Long Papers)*, pages 3828–3850, 2024.
- [31] Rahul K Arora, Jason Wei, Rebecca Soskin Hicks, Preston Bowman, Joaquin Quiñonero-Candela, Foivos Tsimpourlas, Michael Sharman, Meghan Shah, Andrea Vallone, Alex Beutel, et al. Healthbench: Evaluating large language models towards improved human health. *arXiv preprint arXiv:2505.08775*, 2025.
- [32] Dan Hendrycks, Collin Burns, Steven Basart, Andy Zou, Mantas Mazeika, Dawn Song, and Jacob Steinhardt. Measuring massive multitask language understanding. *Proceedings of the International Conference on Learning Representations (ICLR)*, 2021.
- [33] Haonan Li, Yixuan Zhang, Fajri Koto, Yifei Yang, Hai Zhao, Yeyun Gong, Nan Duan, and Timothy Baldwin. Cmmlu: Measuring massive multitask language understanding in chinese. In *Findings of the Association for Computational Linguistics: ACL 2024*, pages 11260–11285, 2024.
- [34] Sandhini Agarwal, Lama Ahmad, Jason Ai, Sam Altman, Andy Applebaum, Edwin Arbus, Rahul K Arora, Yu Bai, Bowen Baker, Haiming Bao, et al. gpt-oss-120b & gpt-oss-20b model card. *arXiv preprint arXiv:2508.10925*, 2025.
- [35] Yaowei Zheng, Richong Zhang, Junhao Zhang, YeYanhan YeYanhan, and Zheyuan Luo. Llamafactory: Unified efficient fine-tuning of 100+ language models. In *Proceedings of the 62nd Annual Meeting of the Association for Computational Linguistics (Volume 3: System Demonstrations)*, pages 400–410, 2024.
- [36] An Yang, Baosong Yang, Binyuan Hui, Bo Zheng, Bowen Yu, Chang Zhou, Chengpeng Li, Chengyuan Li, Dayiheng Liu, Fei Huang, et al. Qwen2 technical report. *arXiv preprint arXiv:2407.10671*, 2024.
- [37] Bowen Zhang, Zixin Song, Chunquan Chen, Qian-Wen Zhang, Di Yin, and Xing Sun. Codiemb: A collaborative yet distinct framework for unified representation learning in information retrieval and semantic textual similarity. *arXiv preprint arXiv:2508.11442*, 2025.
- [38] Zhihong Shao, Peiyi Wang, Qihao Zhu, Runxin Xu, Junxiao Song, Xiao Bi, Haowei Zhang, Mingchuan Zhang, YK Li, Yang Wu, et al. Deepseekmath: Pushing the limits of mathematical reasoning in open language models. *arXiv preprint arXiv:2402.03300*, 2024.
- [39] Ziyang Miao, Qiyu Sun, Jingyuan Wang, Yuchen Gong, Yaowei Zheng, Shiqi Li, and Richong Zhang. Easy dataset: A unified and extensible framework for synthesizing llm fine-tuning data from unstructured documents. In *Proceedings of the 2025 Conference on Empirical Methods in Natural Language Processing: System Demonstrations*, pages 960–968, 2025.
- [40] Jinhyuk Lee, Wonjin Yoon, Sungdong Kim, Donghyeon Kim, Sunkyu Kim, Chan Ho So, and Jaewoo Kang. Biobert: a pre-trained biomedical language representation model for biomedical text mining. *Bioinformatics*, 36(4):1234–1240, 2020.

- [41] Zhenchao Tang, Guanxing Chen, Shouzhi Chen, Jianhua Yao, Linlin You, and Calvin Yu-Chian Chen. Modal-nexus auto-encoder for multi-modality cellular data integration and imputation. *Nature Communications*, 15(1):9021, 2024.
- [42] Krzysztof Polański, Matthew D Young, Zhichao Miao, Kerstin B Meyer, Sarah A Teichmann, and Jong-Eun Park. Bbknn: fast batch alignment of single cell transcriptomes. *Bioinformatics*, 36(3):964–965, 2020.
- [43] Ilya Korsunsky, Nghia Millard, Jean Fan, Kamil Slowikowski, Fan Zhang, Kevin Wei, Yuriy Baglaenko, Michael Brenner, Po-ru Loh, and Soumya Raychaudhuri. Fast, sensitive and accurate integration of single-cell data with harmony. *Nature methods*, 16(12):1289–1296, 2019.
- [44] Gefei Wang, Jia Zhao, Yingxin Lin, Tianyu Liu, Yize Zhao, and Hongyu Zhao. scmodal: a general deep learning framework for comprehensive single-cell multi-omics data alignment with feature links. *Nature Communications*, 16(1):4994, 2025.
- [45] Malte D Luecken, Maren Büttner, Kridsakorn Chaichoompu, Anna Danese, Marta Interlandi, Michaela F Müller, Daniel C Strobl, Luke Zappia, Martin Dugas, Maria Colomé-Tatché, et al. Benchmarking atlas-level data integration in single-cell genomics. *Nature Methods*, 19(1):41–50, 2022.
- [46] Charlotte Bunne, Yusuf Roohani, Yanay Rosen, Ankit Gupta, Xikun Zhang, Marcel Roed, Theo Alexandrov, Mohammed AlQuraishi, Patricia Brennan, Daniel B Burkhardt, et al. How to build the virtual cell with artificial intelligence: Priorities and opportunities. *Cell*, 187(25):7045–7063, 2024.
- [47] Yusuf H Roohani, Tony J Hua, Po-Yuan Tung, Lexi R Bounds, Feiqiao B Yu, Alexander Dobin, Noam Teyssier, Abhinav Adduri, Alden Woodrow, Brian S Plosky, et al. Virtual cell challenge: Toward a turing test for the virtual cell. *Cell*, 188(13):3370–3374, 2025.

A Extended Data Text

A.1 SFT and BFT Training Algorithms

We provide the detailed training procedures for SFT and BFT.

Algorithm 1 Supervised Fine-Tuning (SFT)

```

1: Input: Dataset  $\mathcal{D}$ , initial model  $\pi_\theta$ , batch size  $B$ , learning rate  $\eta$ 
2: while not converged do
3:   Sample mini-batch  $\{(x_b, y_b^*)\}_{b=1}^B \sim \mathcal{D}$ 
4:   for  $b = 1$  to  $B$  do
5:     for  $t = 1$  to  $|y_b^*|$  do
6:        $p_{b,t} \leftarrow \pi_\theta(y_{b,t}^* \mid y_{b,<t}^*, x_b)$  {Token probability}
7:        $\ell_{b,t} \leftarrow -\log p_{b,t}$  {Cross-entropy loss}
8:     end for
9:      $L_b \leftarrow \frac{\sum_t m_{b,t} \ell_{b,t}}{\sum_t m_{b,t} + \varepsilon}$  {Masked sequence loss}
10:  end for
11:   $L \leftarrow \frac{1}{B} \sum_{b=1}^B L_b$ 
12:   $\theta \leftarrow \theta - \eta \nabla_\theta L$  {Gradient update}
13: end while

```

Algorithm 2 Balanced Fine-Tuning (BFT)

```

1: Input: Dataset  $\mathcal{D}$ , model  $\pi_\theta$ , batch size  $B$ , window size  $g$ , learning rate  $\eta$ 
2: while not converged do
3:   Sample mini-batch  $\{(x_b, y_b^*)\}_{b=1}^B \sim \mathcal{D}$ 
4:   for  $b = 1$  to  $B$  do
5:     for  $t = 1$  to  $|y_b^*|$  do
6:        $p_{b,t} \leftarrow \pi_\theta(y_{b,t}^* \mid y_{b,<t}^*, x_b)$ 
7:        $\ell_{b,t} \leftarrow -\log p_{b,t}$ 
8:        $w_{b,t} \leftarrow \text{sg}(p_{b,t})$  {Inherited DFT token weight}
9:     end for
10:    {Sliding-window group confidence (stride = 1)}
11:    for  $i = 1$  to  $|y_b^*| - g + 1$  do
12:       $C_{b,i} \leftarrow \frac{1}{g} \sum_{t=i}^{i+g-1} p_{b,t}$  {Mean probability in window}
13:    end for
14:     $p_b^{\text{conf}} \leftarrow \min_i C_{b,i}$  {Identify weakest link}
15:     $s_b \leftarrow \text{sg}(1 - p_b^{\text{conf}})$  {Sample-level balance coefficient}
16:     $L_b \leftarrow s_b \cdot \frac{\sum_t m_{b,t} w_{b,t} \ell_{b,t}}{\sum_t m_{b,t} + \varepsilon}$  {Dual-scale weighted loss}
17:  end for
18:   $L \leftarrow \frac{1}{B} \sum_{b=1}^B L_b$ 
19:   $\theta \leftarrow \theta - \eta \nabla_\theta L$ 
20: end while

```

B Extended Data Figure

B.1 Training Data Samples

<p>Prompt template:</p> <p>Given the NCBI summary of a gene, please extract 2–3 data points from the summary for SFT. The summary of the current gene is as follows:</p> <p>Gene summary:</p> <p>"TP53": "Official Symbol TP53 provided by HGNC; Official Full Name tumor protein p53; Gene type protein coding; Organism Homo sapiens; Also known as P53, BCC7, LFS1, BMFS5, TRP53. Summary: This gene encodes a tumor suppressor protein containing transcriptional activation, DNA-binding, and oligomerization domains. It responds to diverse cellular stresses to regulate target genes, inducing cell cycle arrest, apoptosis, senescence, DNA repair, and metabolic changes. Mutations are associated with many human cancers, including Li-Fraumeni syndrome. Alternative splicing, alternate promoters, and alternative translation initiation produce multiple transcript variants and isoforms. Expression is ubiquitous, with high levels in spleen (RPKM 13.2) and lymph node (RPKM 13.1)."</p> <p>Sample 1:</p> <pre>{ "instruction": "Summarize the biological function of the TP53 gene.", "output": "TP53 encodes a tumor suppressor protein that maintains genomic stability. It contains transcriptional activation, DNA-binding, and oligomerization domains, and responds to cellular stress by regulating target gene expression. This drives cell cycle arrest, apoptosis, senescence, DNA repair, and metabolic regulation." }</pre> <p>Sample 2:</p> <pre>{ "instruction": "Explain the disease relevance of TP53.", "output": "Mutations in TP53 are associated with numerous human cancers, including hereditary cancer syndromes such as Li-Fraumeni syndrome. These mutations impair tumor suppressor function and contribute to uncontrolled cell growth and tumor development." }</pre> <p>Sample 3:</p> <pre>{ "instruction": "Describe the expression pattern and transcript diversity of TP53.", "output": "TP53 is ubiquitously expressed, with high levels in spleen (RPKM 13.2) and lymph node (RPKM 13.1). The gene undergoes alternative splicing and uses multiple promoters, generating multiple transcript variants and isoforms. Additional isoforms can arise from alternative translation initiation within identical transcripts." }</pre>
--

Figure 6: This case demonstrates how to generate biological training data from an NCBI gene summary.

B.2 Case of SFT and BFT Responses (Gene)

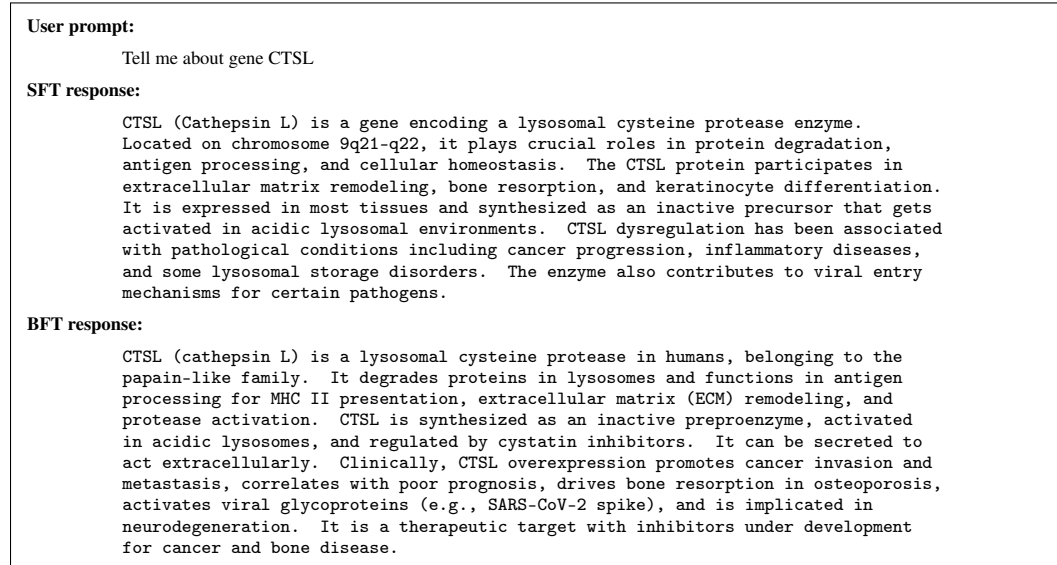


Figure 7: This case examines LLMs' mastery of genetic knowledge.

B.3 Case of SFT and BFT Responses (Biological Process)

User prompt:
Your task is to propose a biological process term for gene sets. Here is the gene set: ZMPSTE24, BANF1, WRN, LMNA.

SFT response:
Process: Suppression of tumor growth via gene silencing. Step 1 (critical analysis): ZMPSTE24 is described as a protein kinase regulating growth via RAS-MAPK; BANF1 as a transcription factor activating cyclin D1/E2; WRN as a non-coding RNA scaffold for RNAi; LMNA as a component of an RNAi complex. Step 2 (functional associations): ZMPSTE24 plus BANF1 are said to promote proliferation, while WRN plus LMNA are said to suppress tumor growth by silencing oncogenes. Step 3 (summary): the dominant process is proposed as suppression of tumor growth via gene silencing.

BFT response:
Process: Nuclear lamina organization and genome stability. Step 1 (critical analysis): ZMPSTE24 is an inner-membrane zinc metalloprotease that processes pre-lamin A; LMNA encodes lamin A/C as structural components of the nuclear lamina; BANF1 links chromatin to LEM-domain proteins and is required for nuclear envelope reassembly; WRN is a RecQ helicase involved in replication, DNA repair, and telomere maintenance. Step 2 (functional associations): ZMPSTE24 directly processes LMNA-derived pre-lamin A; BANF1 couples lamina and chromatin; intact lamina supports genome maintenance; WRN resolves replication stress and DNA lesions; defects converge on progeroid phenotypes. Step 3 (summary): the shared process is maintenance of nuclear lamina structure that safeguards genome stability, i.e., Nuclear lamina organization and genome stability.

Figure 8: This case examines the reasoning ability of LLMs regarding biological processes.

B.4 Workflow of Biological Embedding

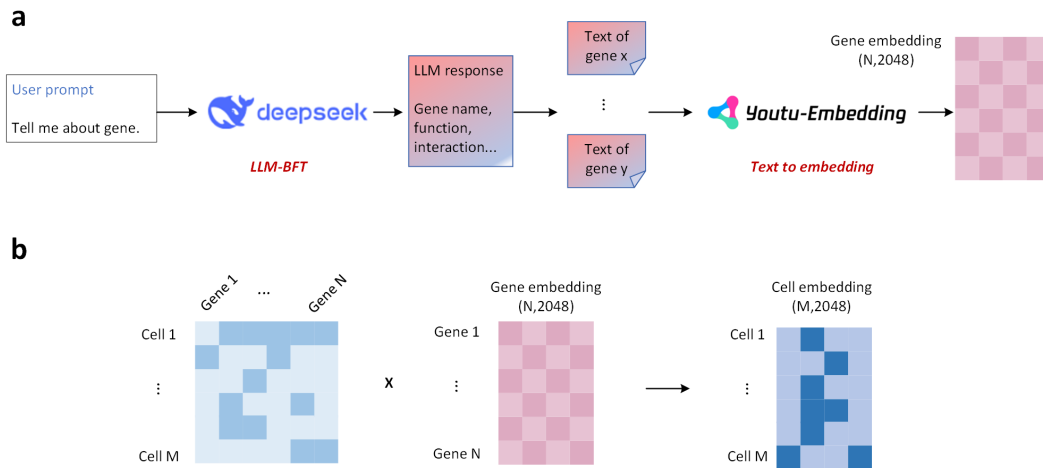


Figure 9: Workflow for extracting biological embeddings from LLM-BFT. **a**: LLM-BFT generates responses based on entities of interest (e.g., a specific gene). The textual description of the gene is input into Tencent Youtu-Embedding to obtain gene embeddings. **b**: For a single-cell dataset, gene embeddings are weighted by gene expression values to generate cell embeddings.

B.5 UMAP of Multi-Gene Task

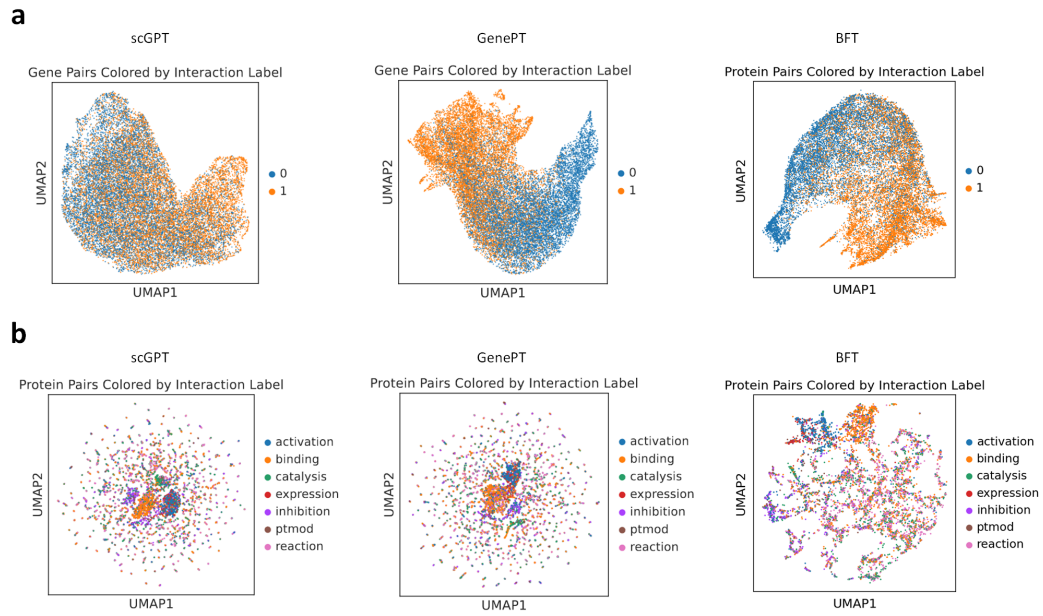


Figure 10: UMAP visualization of the multi-gene input task. **a**: For GGI, the input embedding of the classifier is directly concatenated from the embeddings of two genes. **b**: For PPI, the input embedding of the classifier is directly concatenated from the embeddings of two proteins.

B.6 UMAP of Cell Embedding

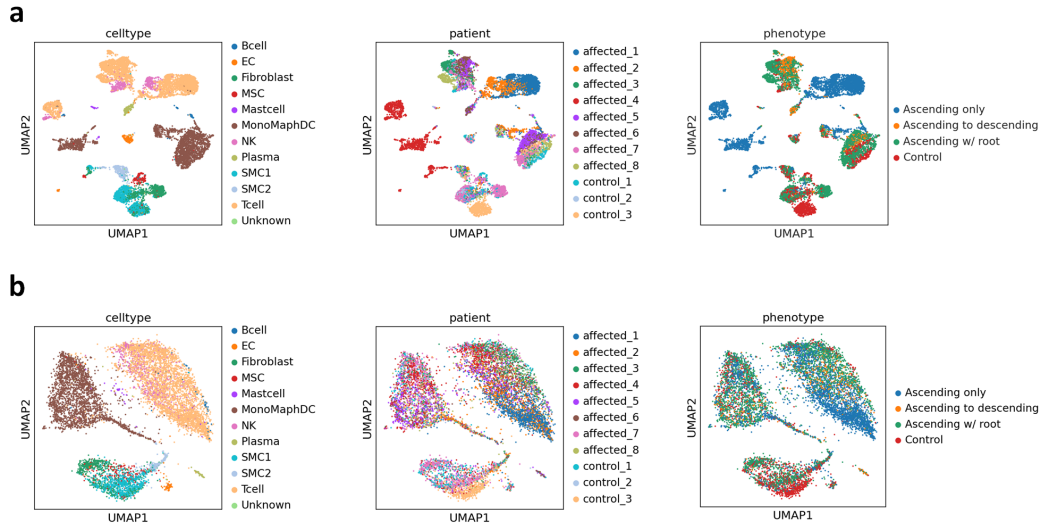


Figure 11: UMAP visualization of cell-level embeddings. **a**: PCA embeddings of the raw data, colored by cell type labels (cell type heterogeneity), patient labels (batch labels), and phenotype labels (disease heterogeneity), respectively. **b**: Cell embeddings derived from LLM-BFT, colored by cell type labels (cell type heterogeneity), patient labels (batch labels), and phenotype labels (disease heterogeneity), respectively.

B.7 UMAP of Multi-Modal Integration

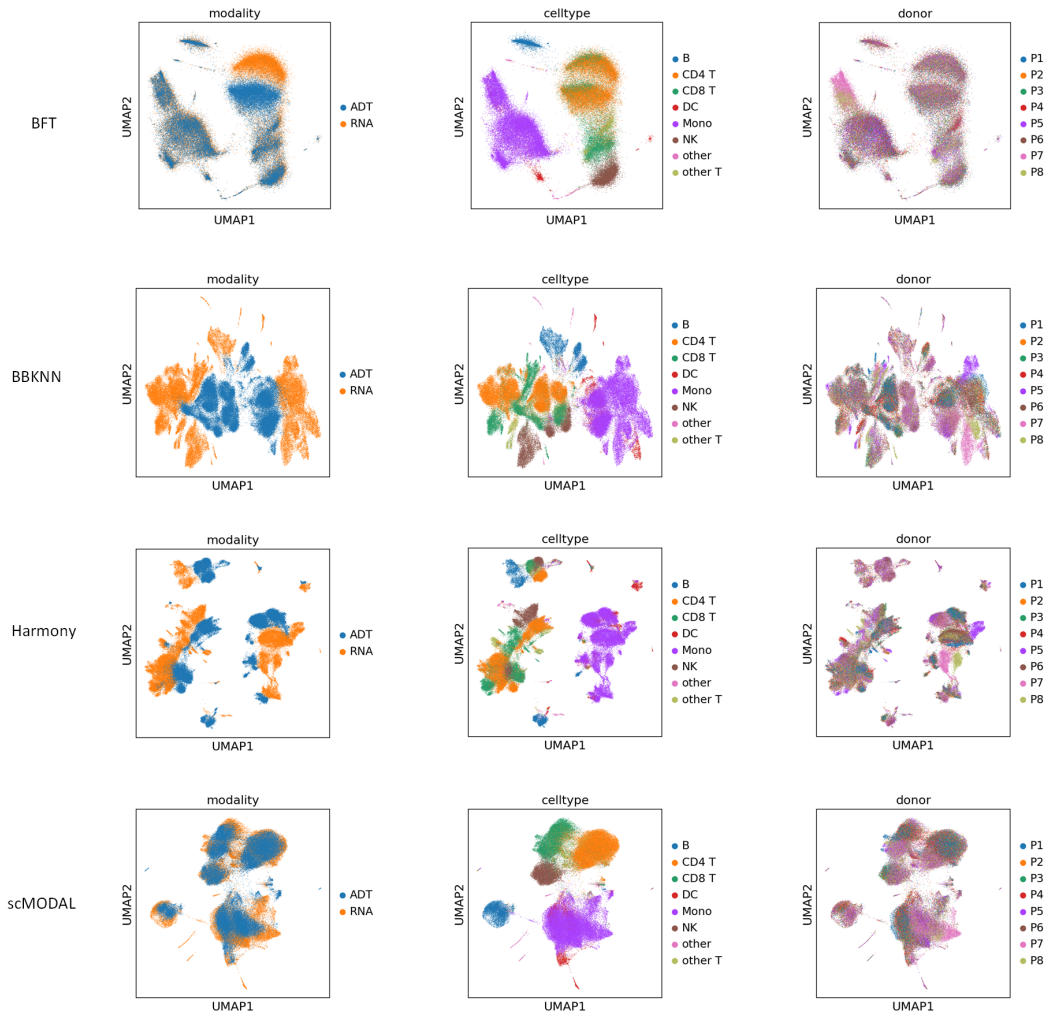


Figure 12: UMAP visualization of single-cell multimodal data integration results. Rows 1 to 4 represent different integration methods, respectively. Columns 1 to 3 correspond to different coloring labels (modality, cell type, and donor), respectively.

B.8 Comparison of Multi-Modal Integration

Method	Bio conservation					Batch correction					Aggregate score		
	Isolated labels	KMeans NMI	KMeans ARI	Silhouette label	cLISI	Silhouette batch	iLISI	KBET	Graph connectivity comparison	PCR comparison	Batch correction	Bio conservation	Total
scMODAL	0.54	0.66	0.53	0.60	1.00	0.87	0.46	0.28	0.69	0.80	0.62	0.67	0.65
BFT	0.52	0.61	0.45	0.54	0.98	0.96	0.34	0.47	0.52	0.20	0.50	0.62	0.57
Harmony	0.48	0.44	0.45	0.54	0.98	0.75	0.08	0.04	0.48	0.56	0.38	0.58	0.50
BBKNN	0.52	0.51	0.40	0.57	0.99	0.48	0.00	0.02	0.45	0.00	0.19	0.60	0.43

Figure 13: Comparison of multimodal integration at the cell level, with the goal of integrating the two modalities of RNA and ADT. The three main columns (Bio conservation, Batch correction, and Aggregate score) respectively represent biological heterogeneity, modality mixing degree, and the overall metric. Each main column contains specific sub-metrics. For the first two columns, the color gradient from purple to green indicates scores from low to high.

B.9 Perturbation Response Prediction

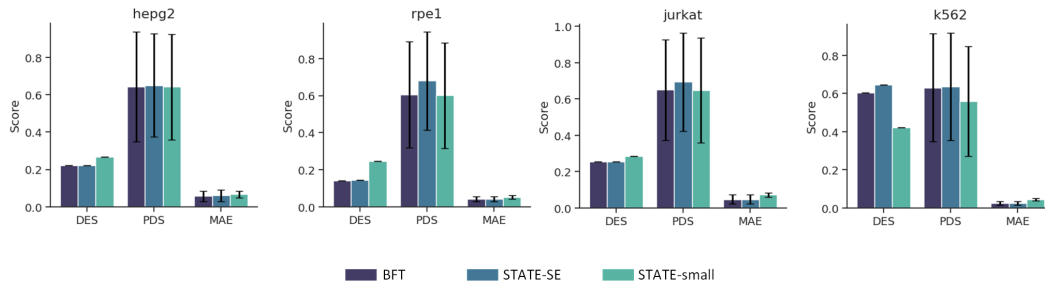


Figure 14: Comparison of single-cell perturbation response prediction results, with zero-shot prediction conducted on four perturbation datasets respectively.

C Extended Data Table

C.1 Group A/B Token Mapping

Table 1: Compact mapping between Group A/B token composition and optimization roles.

Group	Dominant tokens	Minor tokens	Type	Optimization role
Group A (isolated low)	Interchangeable expressions (near-synonymous verbs/adverbs/discourse connectors)	Few ordinary words; very few biomedical entities/reasoning connectives	Aleatoric	Token-level reweighting suppresses unstable gradients from isolated ambiguous choices
Group B (contiguous low window)	Biomedical entities + causal reasoning chains	Few ordinary filler words; very few interchangeable expressions	Epistemic	Sample-level weight $s_b = \text{sg}(1 - p_b^{\text{conf}})$ strengthens knowledge-dense hard-sample learning in a bounded way

C.2 Biomedical Tasks

Table 2: Overview of biomedical tasks evaluated in this study, detailing their biological significance, required knowledge domains, and state-of-the-art (SOTA) baselines.

Task Name (Benchmark)	Biological Significance	Knowledge Required	Current SOTA / Baseline
Medical Reasoning (OpenAI Health Bench [31])	Critical for developing clinical decision support systems. Evaluating on 'Hard' subsets tests reliability in real-world clinical scenarios.	Clinical guidelines, diagnostic logic, symptomatology, and ability to handle ambiguous medical data.	GPT 5.4.
Biological Process Reasoning (GeneAgent [9])	Essential for understanding molecular mechanisms of disease and identifying drug targets. Requires inferring a specific biological pathway from a set of genes.	High-level biological reasoning, understanding of gene-gene relationships, and functional pathway organization.	GeneAgent [9].
Gene Attribute Prediction (GenePT [26])	Predicts intrinsic properties like dosage sensitivity, methylation status (bivalency), and transcription factor range. Crucial for understanding gene regulation and epigenetics.	Epigenetic states, transcriptional regulatory logic, and gene dosage effects.	GenePT [26].
Interaction Prediction (GenePT [26])	Predicts Gene-Gene Interactions (GGI) and Protein-Protein Interactions (PPI). Fundamental for mapping cellular signaling networks and protein complexes.	Physical and functional connectivity between biomolecules; co-expression patterns.	GenePT [26].
Single-cell Multi-modal Integration (Monae [41])	Integrates transcriptomic (RNA) and proteomic (ADT) data. Vital for resolving cellular heterogeneity and creating unified cell atlases.	Cross-modal correlations (Central Dogma: RNA \rightarrow Protein) and noise distribution in single-cell sequencing.	scMODAL [44].
Perturbation Response Prediction (STATE [11])	Predicts how cells change after genetic (CRISPR) or chemical perturbations. Serves as the cornerstone for "Virtual Cell" modeling and in silico drug screening.	Causal gene regulatory networks; dynamic response mechanisms to external stimuli.	STATE [11].

C.3 Comparison of SFT and BFT Responses (Gene)

Table 3: Comparison of SFT and BFT Responses to the "Tell me about gene CTSL" Prompt.

Feature	SFT Response (Less Accurate)	BFT Response (More Accurate)	Summary of Differences
Gene Classification	Lysosomal cysteine protease.	Lysosomal cysteine protease, belonging to the papain-like family.	BFT provides the more precise family information (Papain-like family), which is database-level detail.
Maturation Process	Synthesized as inactive precursor, activated in acidic lysosomes.	Synthesized as inactive preproenzyme, activated in acidic lysosomes, and regulated by cystatin inhibitors.	BFT distinguishes between precursor and preproenzyme, and adds the key regulatory factor (Cystatin).
Immune Function	Involved in antigen processing.	Involved in antigen processing for MHC II presentation.	BFT's description is more specific, clarifying CTSL's exact role in adaptive immunity.
Extracellular Function	Involved in ECM remodeling, bone resorption, and keratinocyte differentiation.	Can be secreted extracellularly and has extracellular activity; promotes bone resorption.	BFT explicitly mentions the important characteristic of "secretion", while SFT only lists extracellular activities.
Disease Association	Associated with cancer progression, inflammatory diseases, and some lysosomal storage disorders.	Overexpression promotes cancer invasion and metastasis, correlates with poor prognosis, and is implicated in neurodegeneration.	BFT's disease description is deeper, including the mechanism (invasion/metastasis) and clinical relevance (poor prognosis), while excluding the vague "lysosomal storage disorders".
Viral Infection Role	Also contributes to viral entry mechanisms for certain pathogens.	Activates viral glycoproteins (e.g., SARS-CoV-2 spike protein), facilitating viral entry.	BFT provides the specific mechanism (glycoprotein activation) and example (SARS-CoV-2 spike protein), which is much more valuable than SFT's general statement.
Therapeutic Potential	Not mentioned.	Is a therapeutic target; inhibitors are under development.	BFT explicitly defines its status as a drug target, a key piece of information missed by SFT.

C.4 Comparison of SFT and BFT Responses (Biological Process)

Table 4: Comparison between BFT, SFT, and Real Research on the biological process reasoning form gene set: ZMPSTE24, BANF1, WRN, LMNA.

Gene	BFT (Correct)	SFT (Incorrect)	Real Research
LMNA	Encodes Lamin A/C, major structural components of the nuclear lamina.	A protein component of the "ininklingia complex" that mediates RNAi.	Encodes Lamin A/C, the primary structural proteins of the nuclear lamina (the 'scaffold' of the nucleus).
ZMPSTE24	A zinc metalloprotease that cleaves pre-lamin A to its mature form.	A protein kinase that regulates cell growth via the RAS-MAPK pathway.	A metalloprotease whose only major known role is to perform the final processing step on pre-lamin A (the LMNA product).
WRN	A RecQ helicase (a protein) involved in DNA repair and telomere maintenance.	A non-coding RNA scaffold for RNA interference (RNAi).	A protein-coding gene. The WRN protein is a DNA helicase essential for DNA repair and genome stability.
BANF1	A DNA-binding protein that bridges chromatin to the nuclear envelope.	A transcription factor that activates genes like cyclin D1/E2.	A structural DNA-binding protein that is essential for nuclear envelope reassembly after mitosis and for anchoring chromatin to the inner nuclear membrane.
Overall Process	Nuclear lamina organization and genome stability.	Suppression of tumor growth via gene silencing.	Maintenance of nuclear envelope integrity and genome stability (This pathway is central to human premature aging syndromes).

C.5 More Gene-Level and Cell-Level Results

Results in Tables 5 and 6 reveal that standard SFT and DFT are fundamentally unsuitable for biological representation, consistently underperforming scGPT and even PCA. DFT exhibits the most severe degradation because its suppression of low-confidence tokens removes critical logical spans and rare entities essential for functional projection. While SFT/DFT produce generic descriptions that lack discriminative power, BFT achieves SOTA performance across all benchmarks and clustering metrics (ARI, AMI, ASW). This superiority is robust across different encoders; while Youtu-Embedding extracts richer features than BioBERT, the performance hierarchy remains unchanged. By adaptively mining hard samples and rescuing epistemic signals, BFT transforms the LLM into a high-fidelity semantic projector capable of bridging micro-scale gene functions to macro-scale cellular identities.

Table 5: Quantitative evaluation of biological representations at the gene level. We compare the performance of embeddings derived from different fine-tuning strategies (SFT, DFT, and BFT) across two text-embedding encoders (Youtu-Embedding and BioBERT). All values are reported as AUC. Bold indicates the best performance in each column.

Encoder	Method	TF Range	Dosage	No-methy	Lys4	GGI	PPI
-	scGPT	0.555	0.859	0.799	0.844	0.638	0.658
-	GenePT	0.582	0.889	0.912	0.941	0.803	0.678
Youtu-Embedding	DFT	0.515	0.812	0.758	0.791	0.595	0.601
	SFT	0.531	0.835	0.772	0.810	0.612	0.624
	BFT (Ours)	0.626	0.911	0.929	0.907	0.827	0.766
BioBERT	DFT	0.502	0.801	0.745	0.782	0.584	0.590
	SFT	0.520	0.824	0.760	0.798	0.601	0.610
	BFT (Ours)	0.608	0.897	0.915	0.892	0.811	0.749

Table 6: Quantitative evaluation of cell-level clustering performance across phenotype and cell type labels. We compare embeddings derived from SFT, DFT, and BFT using Youtu-Embedding and BioBERT encoders against traditional baselines (PCA, scGPT, and GenePT). Bold indicates the best performance in each category.

Encoder	Method	Phenotype Clustering			Cell Type Clustering		
		ARI	AMI	ASW	ARI	AMI	ASW
-	PCA	0.13	0.15	0.010	0.14	0.29	0.030
-	scGPT	0.12	0.12	0.010	0.25	0.33	0.040
-	GenePT	0.12	0.11	0.020	0.31	0.47	0.040
Youtu-Embedding	DFT	0.08	0.10	0.002	0.09	0.20	0.015
	SFT	0.10	0.12	0.005	0.11	0.24	0.020
	BFT (Ours)	0.16	0.24	0.020	0.33	0.59	0.060
BioBERT	DFT	0.07	0.09	0.001	0.08	0.18	0.012
	SFT	0.09	0.11	0.004	0.10	0.22	0.018
	BFT (Ours)	0.15	0.22	0.018	0.31	0.55	0.054